SOFT ROBOTS

Somatosensory actuator based on stretchable conductive photothermally responsive hydrogel

Yusen Zhao[1†], Chiao-Yueh Lo[1†], Lecheng Ruan[2], Chen-Huan Pi[2], Cheolgyu Kim[1], Yousif Alsaid[1], Imri Frenkel[1], Rossana Rico[2], Tsu-Chin Tsao[2], Ximin He[1,3]*

Mimicking biological neuromuscular systems' sensory motion requires the unification of sensing and actuation in a singular artificial muscle material, which must not only actuate but also sense their own motions. These functionalities would be of great value for soft robotics that seek to achieve multifunctionality and local sensing capabilities approaching natural organisms. Here, we report a soft somatosensitive actuating material using an electrically conductive and photothermally responsive hydrogel, which combines the functions of piezoresistive strain/pressure sensing and photo/thermal actuation into a single material. Synthesized through an unconventional ice-templated ultraviolet–cryo-polymerization technique, the homogenous tough conductive hydrogel exhibited a densified conducting network and highly porous microstructure, achieving a unique combination of ultrahigh conductivity (36.8 milisiemens per centimeter, 10^3-fold enhancement) and mechanical robustness, featuring high stretchability (170%), large volume shrinkage (49%), and 30-fold faster response than conventional hydrogels. With the unique compositional homogeneity of the monolithic material, our hydrogels overcame a limitation of conventional physically integrated sensory actuator systems with interface constraints and predefined functions. The two-in-one functional hydrogel demonstrated both exteroception to perceive the environment and proprioception to kinesthetically sense its deformations in real time, while actuating with near-infinite degrees of freedom. We have demonstrated a variety of light-driven locomotion including contraction, bending, shape recognition, object grasping, and transporting with simultaneous self-monitoring. When connected to a control circuit, the muscle-like material achieved closed-loop feedback controlled, reversible step motion. This material design can also be applied to liquid crystal elastomers.

INTRODUCTION

One of the unique capabilities that sets living organisms apart from artificial materials is the ability of living organisms to perceive and manage their motion to adapt to their environment. This is enabled by locally sensing their movement (kinesthetic) and environment (tactile) by proprio-/exteroreceptors to provide somatosensory feedback for effectors through the reflex arch or neuromuscular systems (1). For example, octopi exhibit a highly localized and continuous neural system with nonsegmented arms that can accomplish various tasks, ranging from basic arm shortening/elongation to complex object grasping, shape morphing, and accessing restricted environment (Fig. 1A) (2). One of the ultimate goals for robotics is to demonstrate sensorimotor-like abilities, by mimicking the receptors and effectors in biological somatosensory systems to achieve simultaneous active motion and perception functions. This requires integrating sensors and actuators with non-interfering and matching sensitivity to the deformation range, without compromising the desirable high mechanical flexibility, fast actuation, and real-time sensation. Conventional rigid robots achieve actuation through motors and typically use motion encoders (3, 4), force load cells (5), or cameras for sensing and providing feedback on terrain conditions and locomotive gaits; the use of complex and bulky multi-electronics integration, however, often restricts the motility and miniaturization of these robots.

Soft robots, alternatively, use more processable and conformable soft materials (6, 7) and offer promising opportunities for sensing-actuation unification. Some somatosensory soft robots are capable of not only monitoring the roughness, softness, and temperature of objects but also grasping objects using control algorithms (8–10). Current state-of-the-art soft sensors are based on optical fibers (9, 11, 12), electroluminescent dyes (6), triboelectricity (13), and piezoresistivity (6–8, 10, 14–18), whereas soft actuators are based on the asymmetric expansion (16, 19), pneumatic inflation (20), and hydraulic actuation (21). Defined by their specific working mechanisms, these sensors and actuators are all single-function units, still unable to realize sensation and actuation simultaneously. Therefore, add-on functionalities to soft robots have been used to physically integrate the two individual components by welding (7), three-dimensional (3D) printing (8), embedding (9), or laminating sensors and actuators (22). Fabricating such heterogeneous multimaterial systems typically involve complex integrating processes with multiple molding and lamination steps and complicated connection terminals (8, 16). These physically integrated systems with various material interfaces also have potential stress concentration and adhesion issues (1). In terms of robotic performance, the sensing and actuation functionalities are predefined with constrained flexibility when handling complex dynamic environment.

It would be highly advantageous to develop a multifunctional monolithic material containing chemically integrated sensing and actuation components at the molecular level, rather than the system level (1). Such a somatosensory actuatable material can ideally present intrinsic sensing capability and nonpredefined actuation simultaneously, without potential delamination or sensing/actuation range mismatching associated with physically integrated

[1]Department of Material Science and Engineering, University of California, Los Angeles, Los Angeles, CA 90095, USA. [2]Department of Mechanical and Aerospace Engineering, University of California, Los Angeles, Los Angeles, CA 90095., USA. [3]Califonia Nanosystems Institute, Los Angeles, CA 90095, USA.
*Corresponding author. Email: ximinhe@ucla.edu
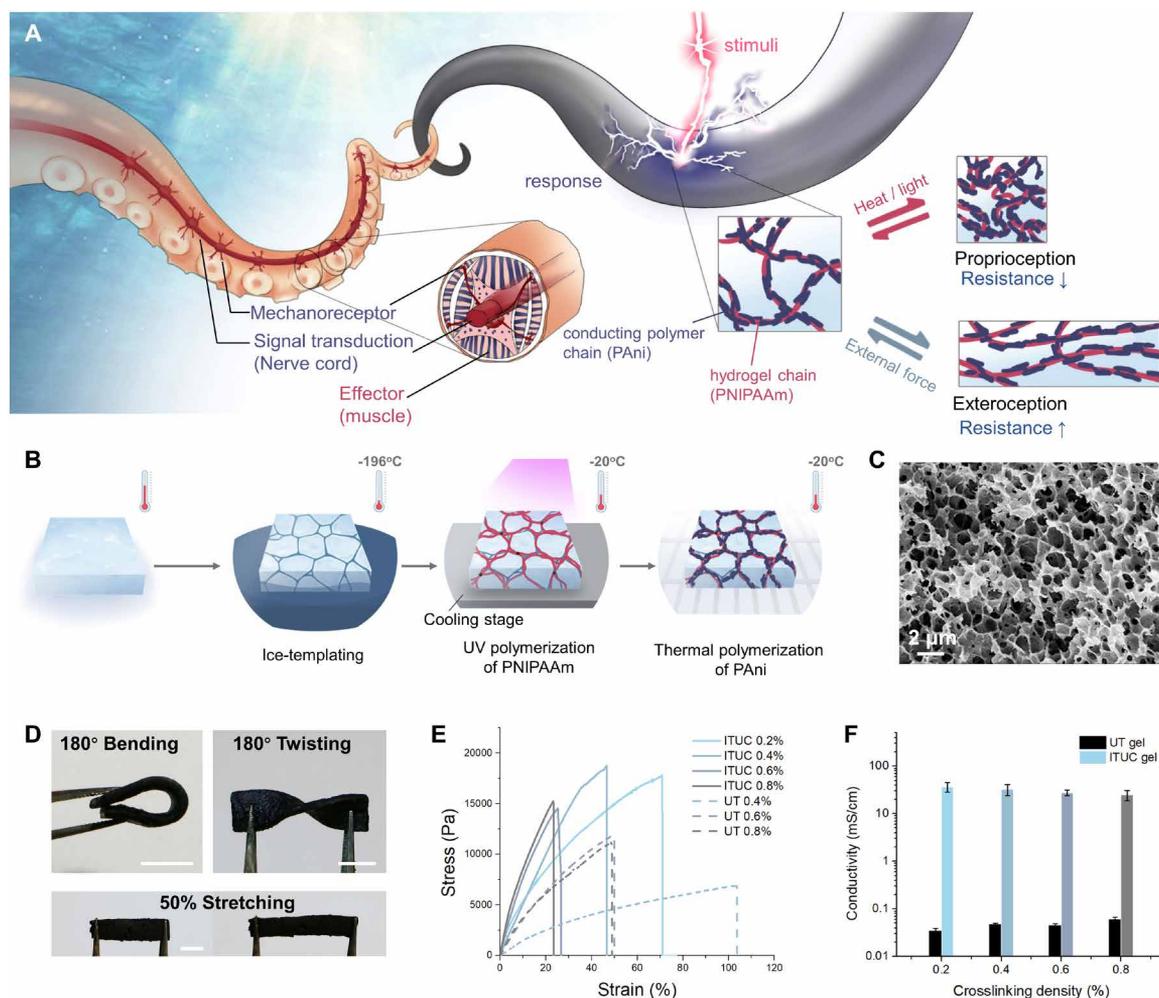†These authors contributed equally to this work.

Fig. 1. Design of the somatosensitive actuator based on CP hydrogel. (**A**) Schematic of the bioinspired self-sensing actuator: Resistance change arose from density change or chain elongation of CP network when exposed to thermal stimulated volumetric change or external stress. (**B**) Fabrication of ITUC gel using the ice-templating, UV polymerization, and cryo-polymerization process. (**C**) SEM image of the ITUC gel. (**D**) Images of ITUC gel during bending, twisting, and stretching. (**E**) Strain-stress curve of the ITUC gel and UT gel (control sample, without ice-templating) with different cross-linking densities. (**F**) Conductivities of the ITUC gels and UT gels.

multiplexed design. In addition, the bulk material with molecularly modular design can be chemically customized and physically tuned for optimized mechanical and electrical properties and further combined with other units for higher-level functionality. However, material designs that seek to accommodate such multifunctionality without a conflict between the signal transductions of the sensing and actuating processes remain limited (*23*). Designing complex energy transduction mechanisms in existing soft materials [e.g., conducting polymers (CPs)] may realize multifunctionality (sensing and actuation); however, the resulting performance would be rather limited and unsatisfactory for the demanding soft robotics applications (e.g., large, fast, and forceful shape changing and high strain sensitivity simultaneously).

Among many active polymers, hydrogels are attractive artificial muscle materials for soft robotics, providing the potential for human-machine interfaces with their 3D hydrophilic polymer networks, mechanical properties similar to biological tissues, and biocompatibility. This class of stimuli-responsive materials can undergo a notable volumetric change in response to a variety of environmental

stimuli (*24–30*) and thus may serve as a good actuator. To manifest the hydrogel's ability to sense, a piezoresistive mechanism is predominantly used, possibly based on ionic or electronic conduction. Whereas ionically conductive materials require low-voltage AC operation due to ion migration, electronic conduction with DC operation (*31*) has advantages with direct readouts to feed the control program for electronic interfaces and for underwater operation without ion leakage issues. Although flexible conductive polymers/hydrogels have been explored for soft electronics applications, these materials lack the stimuli-responsive actuation ability required for soft robotics applications (*32*). Therefore, to prove the concept, we propose that by molecularly combining a stimuli-responsive hydrogel with a CP (*33–35*) in a single material as a model system, both actuation and sensing can be realized simultaneously. The hierarchical porous hydrogel network would allow for both continuous electronic conduction for sensation and efficient mass (water) transport for actuation (*36*). Although CP-percolated stimuli-responsive hydrogels have been reported (*33*), multiple obstacles still remain preventing them from serving as sensory actuators:

(i) CP percolation using conventional two-step methods results in high inhomogeneity, typically with CPs formed only on the hydrogel skin (fig. S2) (37, 38) and is, hence, unable to accurately reflect the actual material deformation. (ii) Creating materials that are both electrically conductive and capable of withstanding large mechanical deformation is a challenge (18, 39). Their conductivity and mechanical robustness are relatively low, due to the formation of nanoaggregation and discontinuities of the two polymer networks, leading to unstable sensing signals (34) and poor actuation and load bearing. (iii) The slow actuation due to the slow diffusion in hydrogels with noncontinuous channels has a response time of minutes or hours (40). (iv) Although the state-of-the-art conductive hydrogels can partially reach high conductivity, good mechanical properties, fast and substantial actuation, or sensing individually, realizing all the desired features simultaneously in a CP-percolated responsive hydrogel composite remains challenging.

Here, we present a soft somatosensitive actuator based on a molecularly innervated CP-percolated hydrogel-based material capable of performing a variety of feedback-controlled robotic tasks, including octopus arm–like shortening, elongation, and object perceiving and grasping. This homogeneous bulk conductive hydrogel is composed of an interpenetrating polymer double-network of poly(N-isopropylacrylamide) (PNIPAAm) and polyaniline (PAni), which combines both photo/thermal actuation and piezoresistive sensing into a monolithic material of "two-in-one" functionality. To achieve the high conductivity and high mechanical robustness necessary for simultaneous optimum strain sensitivity and deformability, we developed an unconventional one-pot synthesis method via the ice-templated, ultraviolet (UV) polymerization of PNIPAAm and cryo-polymerization of PAni (ITUC). It successfully solved the aforementioned three issues with (i) distributing the conductive (sensing) and the stimuli-responsive (actuating) components homogeneously distributed at a molecular level throughout the entire bulk material, (ii) maintaining a continuous pathway for electron conduction and so high sensitivity, while remaining strong and stretchable (a result of the suppressed CP-nanoaggregate overgrowth under subzero reaction and the densified CP packing by ice templating), and (iii) having open pores for high water diffusion and thus fast actuation.

Our material exhibited conductivity enhancements of three orders of magnitude and mechanical modulus enhancement of up to 386%, compared with liquid-phase synthesized hydrogels. As an actuator, the hydrogel can rapidly change to any arbitrary shape and size in response to stimuli and does so with a substantially improved response rate (30-fold faster than conventional PNIPAAm) and a high volume change ratio (shrinkable to 50% volumetrically). We have demonstrated tracking toward incident near-infrared (NIR) light precisely, presenting an autonomous signal-tracking ability with reflex-like, decentralized open-loop feedback and object lifting (20× of its weight) and grasping acting as a soft gripper. As a sensor, exhibiting unique pure ohmic electronic conduction under DC voltage, the hydrogel performed exteroception to detect the mechanical stretching [gauge factor (GF) = $\Delta R/R_0/\varepsilon$ = 2.3 at 170% stretch], bending, and compression. Because this material has noninterfering sensing and actuation (referred as the e-output and photothermal-input), its actuation can be detected in real time to provide sensory feedback, undisturbed by the photothermal activity in actuation. Thus, the sensory actuator also had proprioception to monitor its responsive elongation/shortening and bending/unbending under NIR light stimulation. As a proof of concept, it

was demonstrated that the somatosensitive actuator had the potential to help recognize the shape of an unknown object based on the deformation time and resistance evolution. Furthermore, we developed a closed-loop algorithm for actively controlling the artificial arm elongation/shortening, which could be successfully maintained at targeted lengths precisely. The generality of the modular material design has been demonstrated by successfully realizing CP-percolated liquid crystal elastomer (LCE) material with sensory actuating abilities. Overall, with customizable composition and tunable properties, this class of molecularly innervated somatosensitive active hydrogels successfully takes a step toward next-generation life-like soft robots with a self-diagnostic feedback-controlled autonomy a reality. Meanwhile, they may be applied to and augment current inflatable actuators, prosthetics, exoskeletons, wearable systems, smart textiles, and locomotive robots.

RESULTS

To build a material capable of somatosensitive actuation, we sought out the rational combination of PAni CP and PNIPAAm hydrogel. In this homogeneous interpenetrating polymer network, PNIPAAm provides both thermo-responsive actuating capability and mechanical flexibility, whereas the black-colored conductive PAni simultaneously acts as both a photothermal transductor and a piezoresistive sensor. The resistance change upon material deformation results from the synergic deformation of the PAni network to alter the electrical pathway (41). When temperature increases beyond the lower critical solution temperature (LCST) of PNIPAAm, the resistivity of the hydrogel is substantially reduced as the PAni network becomes more compacted through the marked, temperature-driven shrinkage of PNIPAAm (Fig. 1A) (33, 38).

Fabrication and properties

Traditionally, to obtain a CP-hydrogel composite, a two-step synthesis method has been used. Because of the incompatibility of the two syntheses (42), the hydrogel is formed and subsequently soaked in a CP prepolymer solution to in situ polymerize the CP around existing hydrogel chains (37, 38, 43, 44). However, the submicrometer-sized pores of hydrogels hardly allow for sufficient penetration of CP molecules into the entire hydrogel matrix, which results in a CP-rich shell and a nonconductive core, hindering its application in sensing and actuation (i.e., the ITU in situ gel in fig. S2). To solve the inhomogeneity issue, we designed a one-pot polymerization technique, whereby the PNIPAAm and PAni precursor mixture was first irradiated under UV light to polymerize PNIPAAm and then kept at room temperature overnight to polymerize PAni (fig. S1A). The UV- and thermally polymerized hydrogel, referred to as a UT gel, has uniformly distributed PAni throughout the PNIPAAm network (figs. S2 and S3). We measured the conductivity of the UT gels using the AC impedance method first, to minimize the potential electrical double-layer capacitance (35) due to possible dominant ionic conduction. The conductivities ranged from 0.034 to 0.06 mS/cm at 0.2 to 0.8 weight % (wt %) N,N′-methylenebis(acrylamide) (BIS) cross-linking densities (Fig. 1F). Under DC, however, the resistance of the UT gel (1 cm by 2 cm by 0.1 cm) was still unstable over time and at the scale of 1 megohm, which was close to that of pure water and was therefore unable to accurately reflect the material deformation if it were to serve as a strain sensor. Mechanically, the elastic moduli of the UT gels were 14 to 44 kPa from the tensile

stretching tests (Fig. 1E). Despite the high loading of CP (0.8 M PAni with 20 wt % of PNIPAAm), the resulting conductivity and mechanical properties were relatively low, compared with pure PAni hydrogels (conductivity, 110 mS/cm) (35). This necessitated modification to further boost the conductivity from 10 to 100 mS/cm and the modulus to 0.1 to 1 MPa, to deliver high-performance sensing and powerful actuation. We speculate that the introduction of the nonconducting PNIPAAm and high water content in the polymer matrix might have impeded the conductive pathway. Meanwhile, the liquid-phase polymerization gels suffered from uncontrollable reaction kinetics, leading to the formation of disconnected CP nanoaggregates, and so lacked the desirable compact and interconnected packing needed to ensure continuous electron transport and mechanical strength (42).

To produce dense CP chain packing at micro/nanoscale, we modified the UT synthesis by introducing ice-templating and cryo-polymerization for PAni (Fig. 1B). Specifically, the mixed solution was rapidly frozen under liquid nitrogen (−196°C) to form an ice template, followed by UV- and cryo-polymerization of PNIPAAm and PAni, respectively, in a subzero environment (−20°C). The as-prepared gel is referred to as ITUC gel. The modified ITUC gel was much more robust mechanically, capable of bending freely to 180°, being stretched, and twisted to 180° without causing any material damage (Fig. 1D). From the tensile tests, the ITUC gels with different cross-linking densities (BIS concentrations) showed a tunable tensile strength up to 0.18 MPa and a 250 to 386% modulus enhancement over the UT gels (Fig. 1E). Meanwhile, the ITUC gel with 0.2 wt % BIS presented decent deformability with up to 170% stretch at break, suggesting a broad strain sensing and actuation range. At the same time, the ITUC gels exhibited remarkably high conductivities of 24.6 to 36.8 mS/cm, which were > 10^3 times higher than those of UT gels (Fig. 1F and fig. S4). For more clearly identifying the key factors that enabled the high conductivity, we have also made another two control samples by, respectively, UV–cryo-polymerizing PNIPAAm followed by liquid-state polymerizing PAni from the PNIPAAm-PAni precursor mixture (denoted as ITUL gel), and UV–cryo-polymerizing PNIPAAm followed by immersing in PAni precursor and in situ polymerizing PAni in liquid state as well (denoted as ITU in situ gel) (table S1 and fig. S2). It showed that both the mechanical property and conductivity of the ITUC gel were substantially improved, compared with properties of UT, ITUL, ITU in situ, and literatures using the two-step in situ polymerization methods (figs. S5 and S6). The tremendous enhancement of conductivity can be attributed to the ice densification effect (45) and low-temperature reaction (46, 47) of PAni that allowed for substantially denser packing and effectively mitigated nanoaggregation of PAni, facilitating a continuous electronic pathway (as experimentally compared with ITUL gel with liquid-state polymerization of PAni). The scanning electron microscopy (SEM) images also showed a more compact microstructure with more uniform pore sizes of 0.5 to 2 μm, in contrast with 5- to 10-μm pores of UT gel (fig. S3). Besides, the stability of the ITUC gel constantly soaking in water over time was studied, showing ~46% conductivity drop after a week (fig. S7), which is presumably due to the loss of dopant (phytic acid here) under the long-term neutral pH condition (48). By incorporating polyvinyl alcohol (PVA) in the existing ITUC gel, an improved electronic stability has been achieved (~74% conductivity retention), presumably due to the strong hydrogen bonding of PVA to stabilize the dopant phytic acid (fig. S7).

Actuation performance

To examine the actuation capability of the ITUC hydrogels, we analyzed the hydrogel shrinkage at 40°C and recovery rate at room temperature. The ITUC gel (thickness, 0.1 cm) shrunk up to 49.7% within 1 min, with a diffusion time scale (duration of shrinkage to 1/e of its initial volume) of 8 s (Fig. 2A and fig. S8). Although the hydrogel network was toughened by an ice-induced polymer densification effect, the responsive actuation performance was not notably compromised, compared with the UT gel (fig. S8). Promisingly, the shrinking of the ITUC gel was 10 to 100 times faster than that of the conventional hydrogels on a scale of min (fig. S9) to hours (33, 49). The significantly fast volume changes of our hydrogels arise from the bicontinuous microstructure with open pores, featuring a unique low tortuosity that facilitates rapid water diffusion in and out of the polymeric network (50), and thus swift actuation shown as follows.

The composite hydrogels can be actuated not only by heat but also by light via the photothermal-mechanical mechanism due to the photothermal property of PAni. Under NIR light irradiation, the ITUC gel could effectively shrink and lift a weight of up to 171.6 times of its dry polymer weight (Fig. 2B and movie S1). The hydrogel strip with dimensions of 3.41 mm by 1.36 mm by 7.36 mm can produce a force of 0.055 N and a strength of 10.7 kPa, which is 20 times higher compared with conventional PNIPAAm hydrogels (fig. S10) (51–55). Furthermore, because the composite hydrogels are chemically homogeneous without any composition gradient or interface similar to those in conventional physically integrated systems, they allow for actuation in almost all directions with nearly infinite degrees of freedom. When an NIR light shined on the hydrogel strip at an arbitrary angle, the hydrogel bent toward the incoming light and precisely maintained tracking the light source via real-time autonomous reorientation (Fig. 2C). The hydrogel could rapidly recover its original undeformed configuration when the light was off (Fig. 2D). As depicted in our simulated graphs with our multiphysics model that coupled the photothermal-stress fields in Fig. 2C and movie S2, such a directional, asymmetric motion was attributed to the temperature gradient across the hydrogel (27), where the temperature on the illuminated side increased to above the LCST, whereas the temperature on the shaded side still remained below the LCST, resulting in the local shrinking on the illuminated side and the overall bending of the gel. Once the bending strip reached the light's direction (in that it was parallel to the incident light), it steadily aimed at the incident light controlled by a built-in feedback loop arising from the dynamic light-material interaction. Such an autonomous signal-tracking behavior demonstrated a decentralized, open-loop self-controlled actuation. Apart from the object tracking achieved by the temperature gradient, we also demonstrated that the ITUC gel can bend to a defined direction under elevated temperature through seamlessly adhering the gel with a passive layer in a bimorph assembly (fig. S11). By assembling four hydrogel arms, we successfully fabricated a cross-shape soft gripper, which could rapidly grasp an object in hot water (Fig. 2E and movie S3). This bimorph also showed that the materials can be easily combined with other materials to construct a system for complex tasks.

Sensing performance

The ITUC hydrogel provides high conductivity with stretchability, capable of serving as a piezoresistive strain sensor under
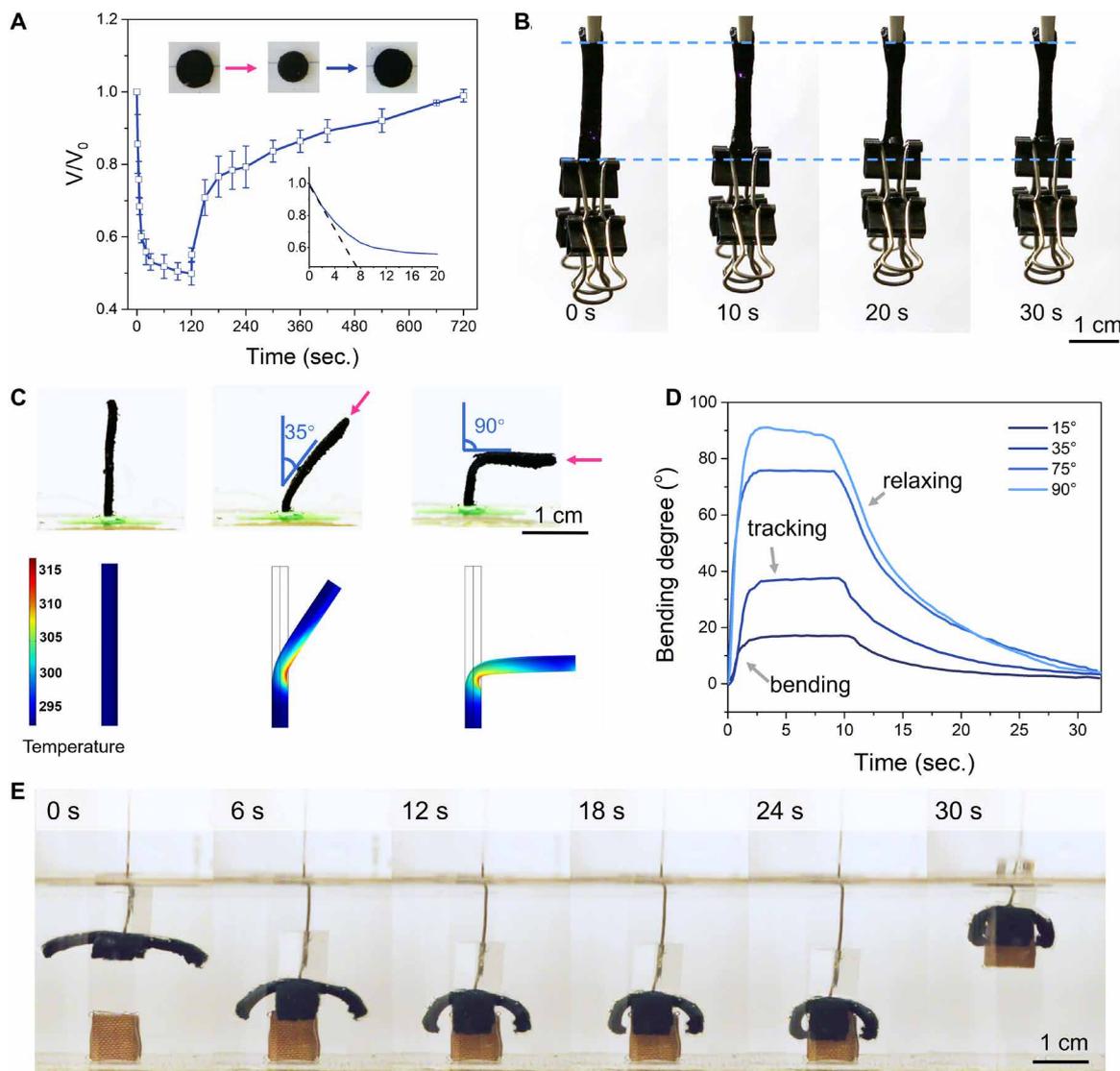
Fig. 2. Actuation performance under thermal or light stimulation. (**A**) Thermal-stimulated volume shrinkage (at 40°C) and recovery (at room temperature) in water. (**B**) Load lifting of ITUC gel under NIR illumination in air. (**C**) Phototropic behavior of ITUC gel that automatically track the light when exposed to a NIR light and the corresponding computer simulation results based on multiphysics model that captured both the bending angle and kinetics. (**D**) The angular evolution of hydrogel tracking to different oblique angles. (**E**) Sequential snapshots of the object grasping using the ITUC gel with a PVA passive layer in 45°C hot water.

mechanical deformation. First, the ITUC gel showed a desirable 0° phase angle at a broad AC frequency range, whereas the UT gel had a >40° phase angle at low frequency (fig. S12). The high phase angle in the UT gel indicated more ionic conduction, leading to the electrochemical reaction at the electrode interface. Second, the ITUC gel showed a desirable <0.4% resistance change over 400 s at direct voltage, in high contrast to the >650,000% large change of the UT gel (Fig. 3B). Furthermore, the current-voltage (*I*-*V*) curve of the ITUC gel was an ideal symmetric straight line, whereas the UT gel showed a capacitive behavior with an enclosed area (Fig. 3C). All these together indicated that the conductivity of the ITUC hydrogel was dominated by ohmic electronic conduction with minor ion-derived conduction, which is highly desired for high sensing performance. This also showed the effectiveness of this new material synthesis method in solving the aforementioned issues of low

electronic conductivity presented by UT gels and conventional conductive gels.

The ITUC gels with high stretchability and responsiveness enabled not only the exteroception to sense passive deformations (Fig. 3D) but also the proprioception to monitor its own motion internally in response to stimulation. For exteroception, we first carried out the strain sensing under uniaxial stretching (Fig. 3D). The GF (GF = $\Delta R/R_0/\varepsilon$, $\Delta R = R - R_0$), which is the relative resistance change to strain ratio, reached 2.3 at 70% tensile strain (Fig. 3D). The sensitivity is comparably higher than PEDOT/PVA and graphene/PAAm gel sensors at the corresponding tensile strain (*34, 56*). The improved sensitivity can be attributed to the uniform continuous CP network without agglomerates by ice-templated low-temperature polymerization. During the passive deformation, the less aggregated microstructure can conformably reflect the macroscopic stretching
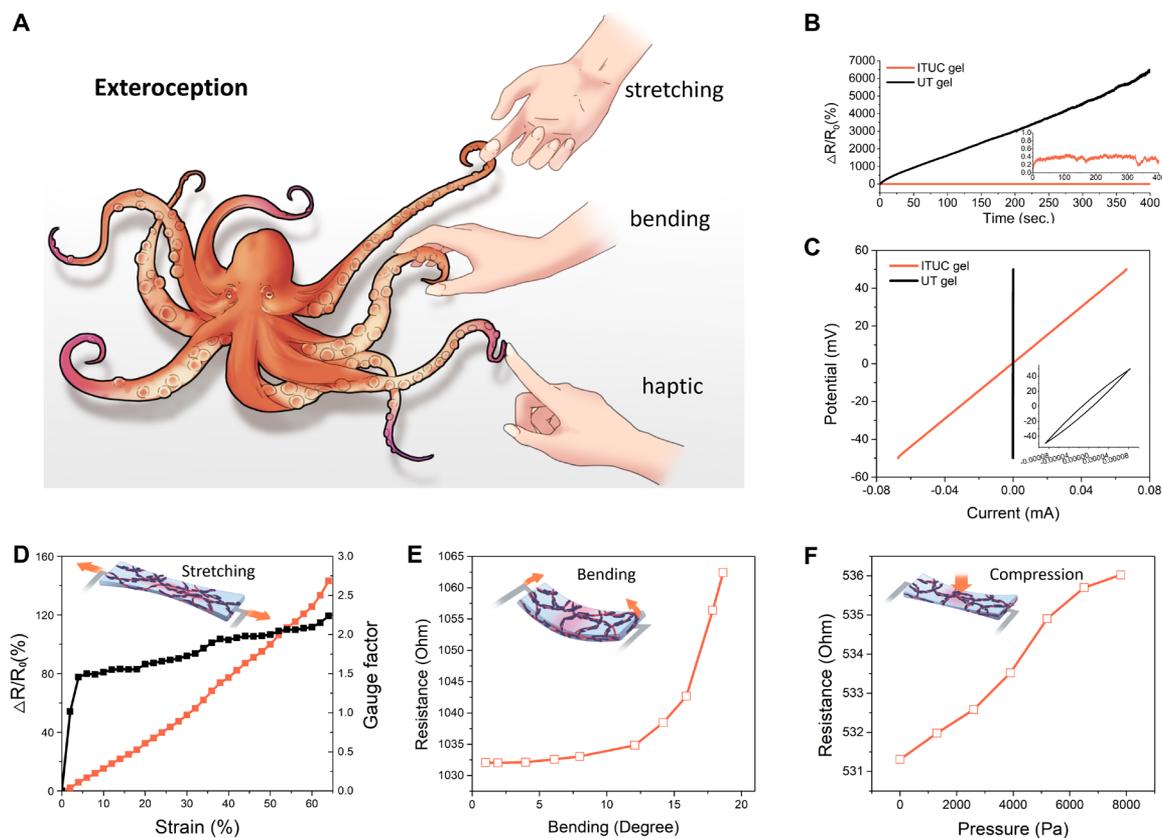
Fig. 3. Exteroceptive sensing of hydrogel. (**A**) Schematic of exteroceptive sensing. (**B**) The resistance of ITUC gel and UT gel over time. The inset shows the zoom-in resistance change for ITUC gel. (**C**) The current-voltage sweep of ITUC gel and UT gel from −50 to 50 mV. (**D**) The resistance change and gauge factor of ITUC gel during stretching. (**E** and **F**) The resistance change of ITUC gel under bending and compression.

of the gel, resulting in higher mechanical robustness and sensory capability (*34*, *56*). Apart from the stretching mode, the hydrogel could also detect the bending and compression, which demonstrates its potential as curvature sensors and haptic (tactile) sensors (Fig. 3, E and F, and figs. S13 and S14). Regarding the similar mechanical properties to biological tissues and compatibility of hydrogels, the ITUC gel can be used for human motion monitoring. The ITUC gel mounted on a human finger could precisely sense the motion of human finger during the bending and recovery at different angles reversibly (fig. S15).

Somatosensitive actuation
Proprioception was further demonstrated through real-time monitoring of its own active actuation behaviors, which mimicked the self-sensing of physical states and motions in living organisms, such as the self-monitored extension or curling of octopus arms. We first demonstrated the kinesthetic shortening/elongation of a hanging ITUC gel by placing a load at the bottom (Fig. 4A and movie S4). Upon illumination by NIR light, the gel strip shortened. The resistance interestingly increased slightly within the first few seconds and then decreased continuously (Fig. 4B). We assume that the initial relative resistance change ($\triangle R/R_0$) spike was ascribed to the rapid microstructural change of PNIPAAm network into clusters that partially isolated the individual PAni chains (*33*). The disconnected clusters resulted in the instant resistance increase in the gel. However, the further shrinkage of the entire dynamic polymer

network enabled well the reconnection of the clusters back to the continuous electron pathway, leading to a continuous resistance decrease. Conversely, as the light was switched off, the resistance was initially reduced over the lower limit, followed by a gradual recovery to the initial state. In addition, we find the design principle to be sufficiently broad for other materials systems, such as liquid crystalline elastomers percolated by CPs. The composites performed similar proprioceptive actuation but much higher generated force due to its nonwater nature (fig. S16).

Similarly, real-time monitoring of photo-responsive bending/unbending actuation was also successfully demonstrated in the hanging gel under unloaded conditions (Fig. 4C and movie S5). Similar light-regulated motion as shown in Fig. 2C was successfully monitored in real time by the gel itself. We noticed slight overbending during its shape recovery upon light shutoff, presumably due to the overheating of the front surface without the restriction of the built-in feedback lock (*26*, *27*). A similar spike in the resistance change was observed within the first few seconds of turning the light on and off caused by the rapid polymer network change (Fig. 4D).

To fully demonstrate the utility of the somatosensory feedback in a soft robotic system, we assembled the ITUC gel into an octopus as a soft proprioceptive arm (Fig. 4E and movie S6). Starting with a straight inactive state, the octopus arm bent up upon NIR illumination and wrapped around a series of cylinders rods of different sizes. The recorded resistance profiles represent the processes of
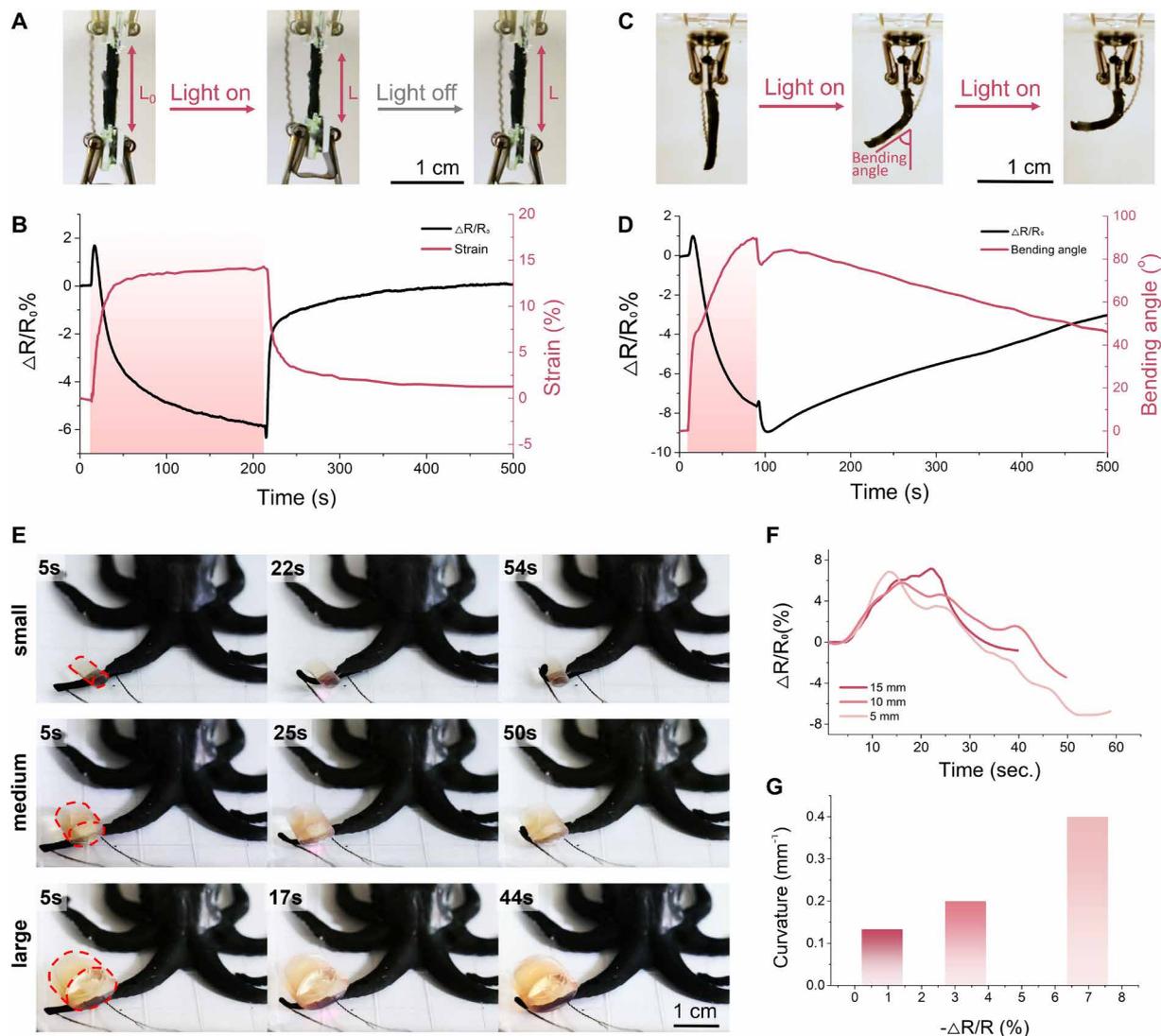
Fig. 4. Proprioceptive sensing of the ITUC gel. (**A**) Proprioceptive shortening and elongation under NIR light. (**B**) Resistance and length change over time. (**C**) Proprioceptive bending and unbending under NIR light. (**D**) Resistance and bending angle over time. (**E**) Shape recognition of an artificial octopus by wrapping the objects and monitoring the resistance. (**F**) Resistance changes of the gel when wrapping different sized objects. (**G**) The correlation of resistance changes and curvatures of objects.

perceiving and grasping the three objects of different diameters respectively (5, 10, and 15 mm; Fig. 4F). Specifically, a 7%-resistance drop occurred when the arm fully wrapped around the 5-mm cylinder, whereas a 0.8% resistance reduction occurred over a relatively shorter period of time when perceiving and grasping the 15-mm cylinder, reflecting the relatively smaller required bending deformation (Fig. 4G). Therefore, both the magnitude and time of resistance change during grasping provide the potential for the shape recognition of unknown objects by the proprioceptive grasping strategy.

Closed-loop actuation

As a key demonstration of the gel's unification of sensory and actuating functions, we developed a closed-loop control system to mimic a biological neuromuscular system, which involves a nerve impulse passing inward from a receptor to the spinal cord and then outward to an effector, much similar to a muscle or gland triggering

an impulsive approach toward or retraction from an external object or environmental stimulus. Control algorithms were designed to precisely regulate the elongation/shortening deformation of a weight-loaded ITUC gel arm, by feeding the controller with the somatosensory feedback pertaining to the real-time length change and controlling the arm shrinking/relaxation motion accordingly (Fig. 5A and movie S7). Specifically, we mounted a gain scheduled bang-bang controller to collect the resistance feedback and correspondingly manipulate the NIR intensity, which successfully held the arm length at three stepwise levels consistently with a 0.16-mm precision ($\Delta L/L_0 = 2.59 \pm 0.66\%$, $5.00 \pm 0.63\%$, and $6.75 \pm 0.60\%$, $L_0 = 25.0$ mm) by controlling relative resistance change ($\Delta R/R_0 = 2.5\%$, 5.0%, and 7.5%) for two stable cycles (Fig. 5B). As shown in Fig. 5 (C and D), both the strip resistance and strain oscillated around the target values in response to the modulation of light intensity. A slight delay in deformation strain change was observed before reaching the equilibrium of the target length when the
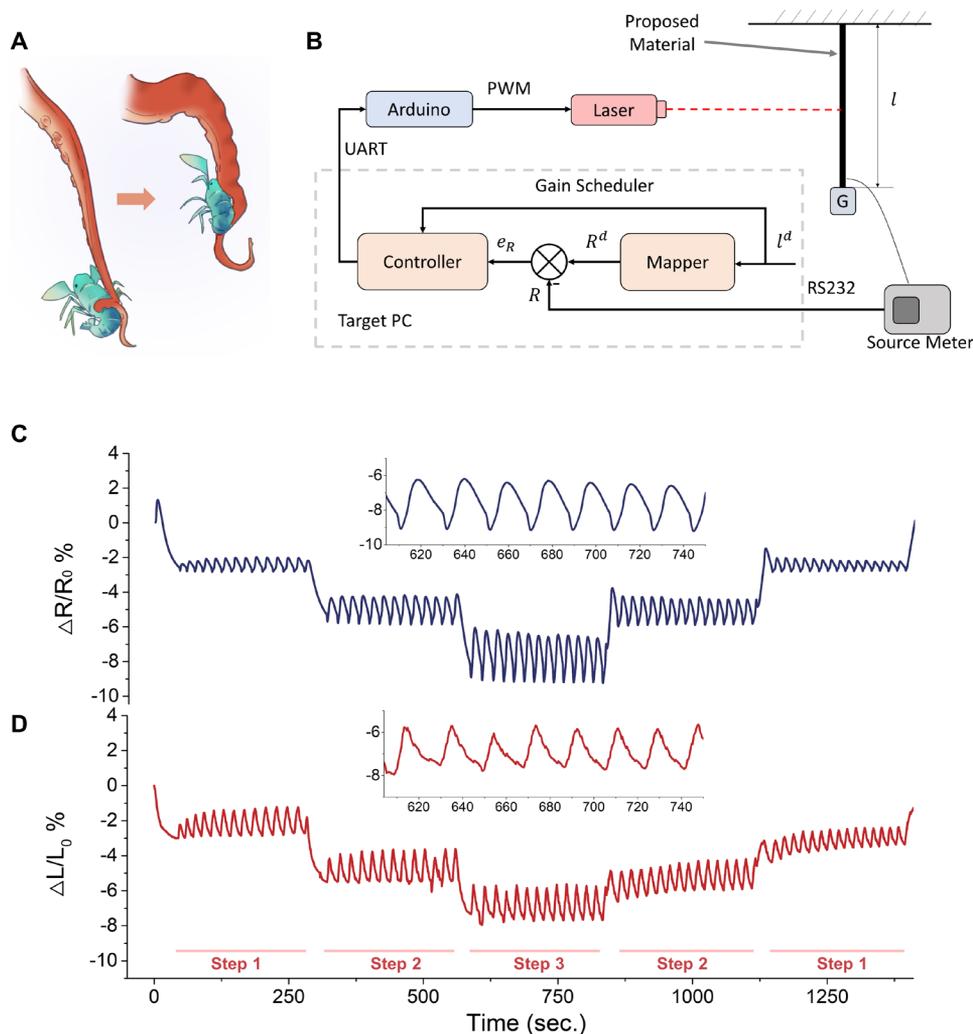
Fig. 5. Closed-loop control setup and performance. (**A**) The schematic of hydrogel arm length shortening control. (**B**) Block diagram of the closed-loop control system. A gain-scheduled bang-bang controller is running on the target personal computer, taking resistance measurements and sending control command via a universal asynchronous receiver-transmitter (UART) to Arduino, which then generates pulse-width-modulation (PWM) signals to drive laser intensity. (**C**) The relative resistance change versus time during closed-loop regulation. (**D**) The corresponding hydrogel arm strain versus time during closed-loop regulation, to stepwise reach the targeted arm lengths at three steps (original length $L_0 = 25.0$ mm, targeted lengths at, respectively, step 1 $L_1 = 24.35$ mm, step 2 $L_2 = 23.75$ mm, and step 3 $L_3 = 23.31$ mm). The insets in (C) and (D) showed the magnified curves between 600 and 750 s and their oscillations at a ~20-s period.

and relaxation more symmetric, which could be attributed to the higher temperature baseline of the sample from continuous illumination. Because the sample kept warm at a temperature close to its LCST, a smaller temperature change and shorter time were required to trigger sample deformation. Consequently, such a smaller light intensity difference upon switching also led to smaller oscillation along the target resistance and deformation.

We have demonstrated the potential of ITUC for closed-loop controlled, self-sensing underwater soft-robotics with stable and stepwise length control with a simple bang-bang controller. On the basis of this proof of concept, the remaining challenges in the calibration curve stability and oscillation amplitude will be addressed through further understanding and optimizing the ITUC hydrogel's stimuli-responsive kinetics and material decay, evaluation of resistance-temperature dependence, and using more delicate control methods such as adaptive control for better performance and more complex robotic tasks.

DISCUSSION
In this work, we successfully demonstrated a proof of the concept for implementing molecularly innervated somatosensitive robotic materials, based on conducting hydrogel composites composed of conductive and responsive polymer networks produced by a one-pot synthesis. The integration of both sensing and actuation functions in a single monolithic material was enabled by the unconventional ice-templated cryo-polymerization strategy, which effectively resolved the long-lasting CP hydrogel challenges in inhomogeneity, aggregation formation, and the resulting low conductivity and poor sensory per-

relative resistance change ramped down (i.e., gel shrinkage going small, during the 870- to 1400-s period), whereas such a delay did not exist during target length ramp-up, attributed to the relatively faster gel shrinkage over its recovery.

The aforementioned abnormal resistance spikes upon strong illumination (Fig. 4B) were observed during the controlled arm elongation steps (fig. S17), but they could be eventually minimized by lowering the light intensity as shown in Fig. 5 (C and D). Meanwhile, the oscillation amplitude could also be suppressed with the effective fine tuning of light intensity when the rapid shrinkage of PNIPAAm network was controlled to occur mildly. It was found that a background nonzero weak illumination substantially increased the response rate and made the resistance responses to the gel shrinking

formance under DC voltage. This material preparation method is universal, capable of coupling broad choices of sensing and actuating functional components into a variety of smart materials. This hybrid material design can not only retain the functionalities from each component but also synergistically achieve high mechanical and electrical properties required for sensory actuation. Compared with conventional multimaterial integrated systems, the somatosensitive actuating material allows for arbitrary sensing location, offers self-contained multiple sensing nodes, and can be custom-designed for broad applications, including the demonstrated basic robotic tasks of contraction, bending, object lifting, and object grasping with open-loop and closed-loop control algorithms. The method can also be used to fabricate miniature robot with multisensory

perception and mobility, which has proved to be a considerable challenge in most current soft robots (*57*).

Our hydrogel system still has several aspects that could be optimized in future investigations: (i) The diffusion-governed response of hydrogel still limits the actuation rate, which can be further improved by morphological or chemical modification, or utilization of other operation mechanism; (ii) in general, the deliverable force of hydrogels is relatively low due to the inherent porous network of high water content, which can be addressed possibly by adding toughening agents; and (iii) obtaining high electrical conduction without compromising high stretchability, achieving high reliability of conduction over time, and stability of piezoresistive sensing mechanism under cyclic operation need to be considered for broader and practical soft robotics applications. Achieving these goals may lead to applications related to remote underwater tasks for marine environments, such as sensing of roughness of an object, controllable gripping soft animals such as mollusks, bypassing an obstacle, and going through a constrained channel. Furthermore, our customizable modular material design can also be extended to other material systems such as LCEs.

From the perspective of the correlation between complexity and functionality of materials systems, we believe that such materials with intrinsic somatosensitive actuating capabilities may open opportunities for intelligent materials with self-regulating functions and computing ability. With further development, this multifunctional material may help advance efforts toward the next generation of soft robots with life-like appearance and performance.

MATERIALS AND METHODS
Materials preparation
Five hundred milligrams of *N*-isopropylacrylamide (NIPAAm); 5, 10, 15, or 20 mg of BIS (0.2, 0.4, 0.6, or 0.8 wt %); 183 μl of purified aniline; 100 μl of Darocur 1173, and a certain amount of dimethyl sulfoxide were mixed into a 2-ml solution, denoted as solution A. Then, 365 mg of ammonium persulfate (APS) was dissolved in 1 ml of water solution. The two solutions were rapidly mixed with the volume ratio of A:B = 4:1 and cast in a mold in contact with liquid nitrogen for freezing. Then, the frozen sample was illuminated under UV light while kept on a −20°C cooling stage. Subsequently, the sample was kept in a −20°C fridge overnight. Last, the sample was taken out to melt and immersed in deionized water to remove excess reactant and salt.

General characterizations
SEM micrographs were taken by Zeiss Supra 40VP SEM. The mechanical properties of hydrogels, including the stress-strain behaviors, were investigated by a dynamic mechanical analyzer (TA Instruments, Q800). The conductivity was measured by attaching two parallel carbon cloth wires as electrodes on the hydrogel film. The AC impedance mode with the frequency sweep from 1 to 100,000 Hz was conducted. The conductivity was calculated according to the formula $\sigma = L/Rwt$, where w and t were the width and thickness of the sample, L was the distance of two carbon cloth, and R was the resistance at 0° phase angle. More than three samples were tested for one experiment.

Actuation and sensing characterization
The swelling and deswelling tests were conducted by placing a round-shape hydrogel in the hot and cold water. The soft gripper was fabricated by growing a chemically cross-linked PVA film on the as-prepared ITUC gel as a passive layer. The exteroceptive sensing tests were carried out by connecting the hydrogel into an electrochemical workstation CHI660E. Strain-sensing experiments were carried out by mounting the hydrogel on a stretching machine (UniVert, CellScale) while connecting the two ends into a circuit. For proprioceptive contraction, bending, and shape recognition, we attached the ITUC gel and electrodes with a clip or the as-mentioned PVA glue.

Closed-loop control of somatosensory actuation
The strain of the hydrogel strip–based artificial arm was measured by its resistance change during the light-triggered shortening and elongation, while being cross-monitored by a digital camera and analyzed with a tracker tool (Open Source Physics Java framework). The standard bang-bang controller algorism was written with Python. The arm length regulation logic is described as below: When the resistance was higher than the target resistance, a stronger light illumination was applied, resulting in arm shortening and thus a drop in resistance. When the resistance was lower than the target resistance, a weaker light illumination was applied, resulting in arm elongation and thus a rise in resistance. The regulation process includes three (A, B, and C) different resistance targets corresponding to the three targeted arm lengths, which are ordered in a stepwise ABCBA manner to demonstrate the ability of reversible arm shortening-elongation regulation.

SUPPLEMENTARY MATERIALS
robotics.sciencemag.org/cgi/content/full/6/53/eabd5483/DC1
Materials, synthesis, characterizations, and closed-loop control
Fig. S1. Schematic of fabrication process of UT gel and ITUC gel.
Fig. S2. Images of hydrogels made by different methods in the cross-sectional view.
Fig. S3. SEM images of UT gels and ITUC gels with different cross-linking densities.
Fig. S4. Phase angles of ITUC gels with different cross-linking densities.
Fig. S5. Mechanical properties and conductivities of the CP-percolated stimuli-responsive hydrogels made by different methods.
Fig. S6. Conductivities and mechanical properties of the CP-percolated stimuli-responsive hydrogels compared with literatures.
Fig. S7. The normalized conductivities of different conductive hydrogels.
Fig. S8. The deswelling rate of UT gels and ITUC gels with different cross-linking densities.
Fig. S9. The deswelling rate of a conventional PNIPAAm hydrogel synthesized in water solution on the scale of minutes.
Fig. S10. The contraction strength and modulus of ITUC gels in comparison with other hydrogels.
Fig. S11. The bending of PVA and ITUC bimorph gel.
Fig. S12. The comparisons of phase angles and real impedance between UT gel and ITUC gel.
Fig. S13. Photographs of exteroceptive bending test.
Fig. S14. Photographs of exteroceptive compression test.
Fig. S15. The application of the ITUC gel as a human motion sensor.
Fig. S16. The demonstration of somatosensitive actuating CP-percolated LCE material.
Fig. S17. Initial performance (before optimization) of the closed-loop controlled elongation/shortening of artificial arm at targeted lengths.
Table S1. Comparison of CP-PNIPAAm hydrogels fabricated by different methods.
Movie S1. Object lifting under NIR light.
Movie S2. Phototropic behavior with computer simulation.
Movie S3. Object grasping in hot water.
Movie S4. Proprioceptive shortening and elongation.
Movie S5. Proprioceptive bending and unbending.
Movie S6. Object shape recognition by proprioceptive grasping.
Movie S7. Closed-loop deformation control demonstration.
References (*58*–*66*)

REFERENCES AND NOTES
1. H. Wang, M. Totaro, L. Beccai, Toward perceptive soft robots: Progress and challenges. *Adv. Sci.* **5**, 1800541 (2018).

2. B. Hochner, An embodied view of octopus neurobiology. *Curr. Biol.* **22**, R887–R892 (2012).

3. T. Mouri, H. Kawasaki, K. Yoshikawa, J. Takai, S. Ito, Anthropomorphic robot hand: Gifu hand III, in *Proceedings of the 2002 International Conference on Control, Automation and Systems (ICCAS 2002)* (2002), pp. 1288–1293.

4. M. C. Carrozza, G. Cappiello, S. Micera, B. B. Edin, L. Beccai, C. Cipriani, Design of a cybernetic hand for perception and action. *Biol. Cybern.* **95**, 629–644 (2006).

5. M. G. Catalano, G. Grioli, E. Farnioli, A. Serio, C. Piazza, A. Bicchi, Adaptive synergies for the design and control of the Pisa/IIT SoftHand. *Int. J. Robot. Res.* **33**, 768–782 (2014).

6. C. Larson, B. Peele, S. Li, S. Robinson, M. Totaro, L. Beccai, B. Mazzolai, R. Shepherd, Highly stretchable electroluminescent skin for optical signaling and tactile sensing. *Science* **351**, 1071–1074 (2016).

7. F. Spina, A. Pouryazdan, J. C. Costa, L. P. Cuspinera, N. Münzenrieder, Directly 3D-printed monolithic soft robotic gripper with liquid metal microchannels for tactile sensing. *Flex. Print. Electron.* **4**, 035001 (2019).

8. R. L. Truby, M. Wehner, A. K. Grosskopf, D. M. Vogt, S. G. M. Uzel, R. J. Wood, J. A. Lewis, Soft somatosensitive actuators via embedded 3D printing. *Adv. Mater.* **30**, 1706383 (2018).

9. H. Zhao, K. O'Brien, S. Li, R. Shepherd, Optoelectronically innervated soft prosthetic hand via stretchable optical waveguides. *Sci. Robot.* **1**, eaai7529 (2016).

10. R. L. Truby, R. K. Katzschmann, J. A. Lewis, D. Rus, in *2019 2nd IEEE International Conference on Soft Robotics (RoboSoft)* (IEEE, 2019), pp. 322–329.

11. C. To, T. L. Hellebrekers, Y. L. Park, in *IEEE/RSJ International Conference on Intelligent Robots and Systems (IROS)* (IEEE, 2015), pp. 5898–5903.

12. H. Zhao, J. Jalving, R. Huang, R. Knepper, A. Ruina, R. Shepherd, A helping hand: Soft orthosis with integrated optical strain sensors and EMG control. *IEEE Robot. Autom. Mag.* **23**, 55–64 (2016).

13. X. Yuan, J. Zou, L. Sun, H. Liu, G. Jin, in *Proceedings of the 2019 International Conference on Robotics, Intelligent Control and Artificial Intelligence* (Association for Computing Machinery, 2019), pp. 690–695.

14. X. Fang, Z. Liu, Y. Hao, H. Yang, J. Liu, Z. Xie, L. Wen, in *2019 2nd IEEE International Conference on Soft Robotics (RoboSoft)* (IEEE, 2019), pp. 25–30.

15. K. Elgeneidy, N. Lohse, M. Jackson, Bending angle prediction and control of soft pneumatic actuators with embedded flex sensors—A data-driven approach. *Mechatronics* **50**, 234–247 (2018).

16. M. Amjadi, M. Sitti, Self-sensing paper actuators based on graphite–carbon nanotube hybrid films. *Adv. Sci.* **5**, 1800239 (2018).

17. S. Wei, L. Zhang, C. Li, S. Tao, B. Ding, H. Zhu, S. Xia, Preparation of soft somatosensory-detecting materials *via* selective laser sintering. *J. Mater. Chem. C* **7**, 6786–6794 (2019).

18. M. D. Dickey, Stretchable and soft electronics using liquid metals. *Adv. Mater.* **29**, 1606425 (2017).

19. H. Cheng, F. Zhao, J. Xue, G. Shi, L. Jiang, L. Qu, One single graphene oxide film for responsive actuation. *ACS Nano* **10**, 9529–9535 (2016).

20. D. Yang, M. S. Verma, J.-H. So, B. Mosadegh, C. Keplinger, B. Lee, F. Khashai, E. Lossner, Z. Suo, G. M. Whitesides, Buckling pneumatic linear actuators inspired by muscle. *Adv. Mater. Technol.* **1**, 1600055 (2016).

21. H. Yuk, S. Lin, C. Ma, M. Takaffoli, N. X. Fang, X. Zhao, Hydraulic hydrogel actuators and robots optically and sonically camouflaged in water. *Nat. Commun.* **8**, 14230 (2017).

22. H. A. Sonar, A. P. Gerratt, S. P. Lacour, J. Paik, Closed-loop haptic feedback control using a self-sensing soft pneumatic actuator skin. *Soft Robot.* **7**, 22–29 (2020).

23. K. Kruusamäe, A. Punning, A. Aabloo, K. Asaka, in *Actuators* (Multidisciplinary Digital Publishing Institute, 2015), vol. 4, pp. 17–38.

24. L. Chen, M. Liu, L. Lin, T. Zhang, J. Ma, Y. Song, L. Jiang, Thermal-responsive hydrogel surface: Tunable wettability and adhesion to oil at the water/solid interface. *Soft Matter* **6**, 2708–2712 (2010).

25. X. B. Zhang, C. L. Pint, M. H. Lee, B. E. Schubert, A. Jamshidi, K. Takei, H. Ko, A. Gillies, R. Bardhan, J. J. Urban, M. Wu, R. Fearing, A. Javey, Optically- and thermally-responsive programmable materials based on carbon nanotube-hydrogel polymer composites. *Nano Lett.* **11**, 3239–3244 (2011).

26. Y. Zhao, C. Xuan, X. Qian, Y. Alsaid, M. Hua, L. Jin, X. He, Soft phototactic swimmer based on self-sustained hydrogel oscillator. *Sci. Robot.* **4**, eaax7112 (2019).

27. X. Qian, Y. Zhao, Y. Alsaid, X. Wang, M. Hua, T. Galy, H. Gopalakrishna, Y. Yang, J. Cui, N. Liu, M. Marszewski, L. Pilon, H. Jiang, X. He, Artificial phototropism for omnidirectional tracking and harvesting of light. *Nat. Nanotechnol.* **14**, 1048–1055 (2019).

28. D. Schmaljohann, Thermo- and pH-responsive polymers in drug delivery. *Adv. Drug Deliv. Rev.* **58**, 1655–1670 (2006).

29. S. K. De, N. R. Aluru, B. Johnson, W. C. Crone, D. J. Beebe, J. Moore, Equilibrium swelling and kinetics of pH-responsive hydrogels: Models, experiments, and simulations. *J. Microelectromech. Syst.* **11**, 544–555 (2002).

30. A. Matsumoto, R. Yoshida, K. Kataoka, Glucose-responsive polymer gel bearing phenylborate derivative as a glucose-sensing moiety operating at the physiological pH. *Biomacromolecules* **5**, 1038–1045 (2004).

31. G. Cai, J. Wang, K. Qian, J. Chen, S. Li, P. S. Lee, Extremely stretchable strain sensors based on conductive self-healing dynamic cross-links hydrogels for human-motion detection. *Adv. Sci.* **4**, 1600190 (2017).

32. Y. Zhao, B. Zhang, B. Yao, Y. Qiu, Z. Peng, Y. Zhang, Y. Alsaid, I. Frenkel, K. Youssef, Q. Pei, X. He, Hierarchically structured stretchable conductive hydrogels for high-performance wearable strain sensors and supercapacitors. *Matter* **3**, 1196–1210 (2020).

33. Y. Shi, C. Ma, L. Peng, G. Yu, Conductive "smart" hybrid hydrogels with PNIPAM and nanostructured conductive polymers. *Adv. Funct. Mater.* **25**, 1219–1225 (2015).

34. Y.-Y. Lee, H.-Y. Kang, S. H. Gwon, G. M. Choi, S.-M. Lim, J.-Y. Sun, Y.-C. Joo, A strain-insensitive stretchable electronic conductor: PEDOT: PSS/acrylamide organogels. *Adv. Mater.* **28**, 1636–1643 (2016).

35. L. Pan, G. Yu, D. Zhai, H. R. Lee, W. Zhao, N. Liu, H. Wang, B. C.-K. Tee, Y. Shi, Y. Cui, Z. Bao, Hierarchical nanostructured conducting polymer hydrogel with high electrochemical activity. *Proc. Natl. Acad. Sci. U.S.A.* **109**, 9287–9292 (2012).

36. Y. Shi, L. Peng, Y. Ding, Y. Zhao, G. Yu, Nanostructured conductive polymers for advanced energy storage. *Chem. Soc. Rev.* **44**, 6684–6696 (2015).

37. K. Wang, X. Zhang, C. Li, X. Sun, Q. Meng, Y. Ma, Z. Wei, Chemically crosslinked hydrogel film leads to integrated flexible supercapacitors with superior performance. *Adv. Mater.* **27**, 7451–7457 (2015).

38. H. Kim, K. Kim, S. J. Lee, Nature-inspired thermo-responsive multifunctional membrane adaptively hybridized with PNIPAm and PPy. *NPG Asia Mater.* **9**, e445 (2017).

39. A. Chortos, J. Liu, Z. Bao, Pursuing prosthetic electronic skin. *Nat. Mater.* **15**, 937–950 (2016).

40. M. C. Koetting, J. T. Peters, S. D. Steichen, N. A. Peppas, Stimulus-responsive hydrogels: Theory, modern advances, and applications. *Mater. Sci. Eng. R Rep.* **93**, 1–49 (2015).

41. J. Teixeira, L. Horta-Romarís, M.-J. Abad, P. Costa, S. Lanceros-Méndez, Piezoresistive response of extruded polyaniline/(styrene-butadiene-styrene) polymer blends for force and deformation sensors. *Mater. Des.* **141**, 1–8 (2018).

42. C. Hu, Y. Zhang, X. Wang, L. Xing, L. Shi, R. Ran, Stable, strain-sensitive conductive hydrogel with antifreezing capability, remoldability, and reusability. *ACS Appl. Mater. Interfaces* **10**, 44000–44010 (2018).

43. Y. Guo, K. Zheng, P. Wan, A flexible stretchable hydrogel electrolyte for healable all-in-one configured supercapacitors. *Small* **14**, 1704497 (2018).

44. K. Sun, E. Feng, G. Zhao, H. Peng, G. Wei, Y. Lv, G. Ma, A single robust hydrogel film based integrated flexible supercapacitor. *ACS Sustainable Chem. Eng.* **7**, 165–173 (2018).

45. J. Lu, H. Wang, Z. Tian, Y. Hou, H. Lu, Cryopolymerization of 1, 2-dithiolanes for the facile and reversible grafting-from synthesis of protein–polydisulfide conjugates. *J. Am. Chem. Soc.* **142**, 1217–1221 (2020).

46. P. C. Maity, M. Khandelwal, Synthesis time and temperature effect on polyaniline morphology and conductivity. *Am. J. Mater. Synt. Process.* **1**, 37–42 (2016).

47. P. N. Adams, P. J. Laughlin, A. P. Monkman, A. M. Kenwright, Low temperature synthesis of high molecular weight polyaniline. *Polymer* **37**, 3411–3417 (1996).

48. D. Mawad, C. Mansfield, A. Lauto, F. Perbellini, G. W. Nelson, J. Tonkin, S. O. Bello, D. J. Carrad, A. P. Micolich, M. M. Mahat, J. Furman, D. Payne, A. R. Lyon, J. J. Gooding, S. E. Harding, C. M. Terracciano, M. M. Stevens, A conducting polymer with enhanced electronic stability applied in cardiac models. *Sci. Adv.* **2**, e1601007 (2016).

49. T. Gan, Y. Guan, Y. Zhang, Thermogelable PNIPAM microgel dispersion as 3D cell scaffold: Effect of syneresis. *J. Mater. Chem.* **20**, 5937–5944 (2010).

50. H. Bai, A. Polini, B. Delattre, A. P. Tomsia, Thermoresponsive composite hydrogels with aligned macroporous structure by ice-templated assembly. *Chem. Mater.* **25**, 4551–4556 (2013).

51. Y. S. Kim, M. Liu, Y. Ishida, Y. Ebina, M. Osada, T. Sasaki, T. Hikima, M. Takata, T. Aida, Thermoresponsive actuation enabled by permittivity switching in an electrostatically anisotropic hydrogel. *Nat. Mater.* **14**, 1002–1007 (2015).

52. Y. Takashima, S. Hatanaka, M. Otsubo, M. Nakahata, T. Kakuta, A. Hashidzume, H. Yamaguchi, A. Harada, Expansion–contraction of photoresponsive artificial muscle regulated by host–guest interactions. *Nat. Commun.* **3**, 1270 (2012).

53. E. Palleau, D. Morales, M. D. Dickey, O. D. Velev, Reversible patterning and actuation of hydrogels by electrically assisted ionoprinting. *Nat. Commun.* **4**, 2257 (2013).

54. L.-W. Xia, R. Xie, X.-J. Ju, W. Wang, Q. Chen, L.-Y. Chu, Nano-structured smart hydrogels with rapid response and high elasticity. *Nat. Commun.* **4**, 2226 (2013).

55. C. Cvetkovic, R. Raman, V. Chan, B. J. Williams, M. Tolish, P. Bajaj, M. S. Sakar, H. H. Asada, M. T. A. Saif, R. Bashir, Three-dimensionally printed biological machines powered by skeletal muscle. *Proc. Natl. Acad. Sci. U.S.A.* **111**, 10125–10130 (2014).

56. H. Zhang, W. Niu, S. Zhang, Extremely stretchable, stable, and durable strain sensors based on double-network organogels. *ACS Appl. Mater. Interfaces* **10**, 32640–32648 (2018).

57. J. Hughes, U. Culha, F. Giardina, F. Guenther, A. Rosendo, F. Iida, Soft manipulators and grippers: A review. *Front. Robot. AI* **3**, 69 (2016).

58. R. E. Rivero, M. A. Molina, C. R. Rivarola, C. A. Barbero, Pressure and microwave sensors/actuators based on smart hydrogel/conductive polymer nanocomposite. *Sens. Actuators B* **190**, 270–278 (2014).

59. Z. Deng, Y. Guo, P. X. Ma, B. Guo, Rapid thermal responsive conductive hybrid cryogels with shape memory properties, photothermal properties and pressure dependent conductivity. *J. Colloid Interface Sci.* **526**, 281–294 (2018).

60. Y. Zhu, S. Liu, X. Shi, D. Han, F. Liang, A thermally responsive host–guest conductive hydrogel with self-healing properties. *Mater. Chem. Front.* **2**, 2212–2219 (2018).

61. W. Hong, X. Zhao, J. Zhou, Z. Suo, A theory of coupled diffusion and large deformation in polymeric gels. *J. Mech. Phys. Solids* **56**, 1779–1793 (2008).

62. W. Hong, Z. Liu, Z. Suo, Inhomogeneous swelling of a gel in equilibrium with a solvent and mechanical load. *Int. J. Solids Struct.* **46**, 3282–3289 (2009).

63. P. J. Flory, J. Rehner Jr., Statistical mechanics of cross-linked polymer networks I. Rubberlike elasticity. *J. Chem. Phys.* **11**, 512–520 (1943).

64. J. Zhang, X. Zhao, Z. Suo, H. Jiang, A finite element method for transient analysis of concurrent large deformation and mass transport in gels. *J. Appl. Phys.* **105**, 093522 (2009).

65. Z. Duan, J. Zhang, J. An, H. Jiang, Simulation of the transient behavior of gels based on an analogy between diffusion and heat transfer. *J. Appl. Mech.* **80**, 041017 (2013).

66. R. P. Feynman, R. B. Leighton, M. Sands, The feynman lectures on physics; vol. i. *Am. J. Phys.* **33**, 750–752 (1965).

Citation: Y. Zhao, C.-Y. Lo, L. Ruan, C.-H. Pi, C. Kim, Y. Alsaid, I. Frenkel, R. Rico, T.-C. Tsao, X. He, Somatosensory actuator based on stretchable conductive photothermally responsive hydrogel. *Sci. Robot.* **6**, eabd5483 (2021).

Science Robotics

Somatosensory actuator based on stretchable conductive photothermally responsive hydrogel

Yusen Zhao, Chiao-Yueh Lo, Lecheng Ruan, Chen-Huan Pi, Cheolgyu Kim, Yousif Alsaid, Imri Frenkel, Rossana Rico, Tsu-Chin Tsao and Ximin He

ARTICLE TOOLS	http://robotics.sciencemag.org/content/6/53/eabd5483
SUPPLEMENTARY MATERIALS	http://robotics.sciencemag.org/content/suppl/2021/04/05/6.53.eabd5483.DC1
REFERENCES	This article cites 60 articles, 4 of which you can access for free http://robotics.sciencemag.org/content/6/53/eabd5483#BIBL
PERMISSIONS	http://www.sciencemag.org/help/reprints-and-permissions

Use of this article is subject to the Terms of Service